

Multiple scattering effects in Doppler optical coherence tomography of flowing blood

J Kalkman¹, A V Bykov², G J Streekstra¹ and T G van Leeuwen^{1,3}

¹ Biomedical Engineering & Physics, Academic Medical Center, University of Amsterdam, PO Box 22700, 1100 DE Amsterdam, The Netherlands

² Optoelectronics and measurement techniques laboratory, University of Oulu, PO Box 4500, 90014 Oulu, Finland

³ Biomedical Photonic Imaging, MIRA Institute for Biomedical Technology and Technical Medicine, University of Twente, PO Box 217, 7500 AE Enschede, The Netherlands

E-mail: j.kalkman@amc.nl

Received 12 December 2011, in final form 30 January 2012

Published 16 March 2012

Online at stacks.iop.org/PMB/57/1907

Abstract

We investigate the effect of multiple scattering on the optical coherence tomography (OCT) signal and the Doppler OCT signal of flowing blood. Doppler OCT measurements at 1300 nm are performed on flowing diluted porcine blood with hematocrit ranging between 0% and 15%. Measured blood hematocrit and mean red blood cell volume are used to calculate, using the discrete dipole approximation model, the (single) scattering coefficient and scattering anisotropy of blood. Monte Carlo simulations, based on the calculated scattering coefficients and scattering anisotropies, are compared to Doppler OCT measurements for hematocrit smaller than 10%. Good quantitative agreement between Doppler OCT measurements and Monte Carlo simulations is observed. Our measurements, calculations and simulations explain the relatively low attenuation coefficients and well preserved flow profiles measured with Doppler OCT for flowing blood. Monte Carlo simulations demonstrate the effect of the scattering anisotropy of the medium on the strength of multiple scattering effects in Doppler OCT signals. With increasing scattering anisotropy the OCT attenuation decreases; the distortion of the flow profile is strongest at intermediate scattering anisotropies (≈ 0.6).

(Some figures may appear in colour only in the online journal)

1. Introduction

Accurate *in vivo* measurement of blood oxygenation and blood flow gives essential clinical indications of the perfusion of tissues. Optical coherence tomography (OCT) is a non-invasive technique that can make high-resolution images of tissue morphology and vasculature up to a few millimeters deep (Huang *et al* 2010). In addition, Doppler OCT is used to quantitatively

measure blood flow by measuring the Doppler shift of light backscattered from red blood cells (RBCs) (Chen *et al* 1997). For low scattering media, the single scattering model provides a good description of both the OCT attenuation (Izatt *et al* 1994) and the Doppler OCT flow in depth. For highly scattering media, deviations of the OCT attenuation from this model are observed: the OCT attenuation coefficient is lower than the (single) scattering coefficient of the medium, and the OCT attenuation coefficient increases nonlinearly with concentration, which are attributed to multiple and concentration-dependent scattering, respectively. These effects have been observed for Intralipid (Kalkman *et al* 2010), a medium with a low scattering anisotropy, and for blood (Faber and van Leeuwen 2009), a medium with a very high scattering anisotropy. Also, for Doppler OCT measurements on flowing Intralipid, multiple scattering effects have been observed in the measured flow profile (Kalkman *et al* 2010). Since these measurements were performed on a medium with a relatively low scattering coefficient, multiple scattering effects on the Doppler OCT flow are rather small. Since blood has a very high scattering coefficient, it is expected that multiple scattering effects are strong and its effect on the Doppler OCT signal is significant.

Multiple scattering effects in OCT have been studied using Monte Carlo (MC) simulations and showed a degradation of the performance of OCT systems. For example, depth ranging, spatial resolution and signal attenuation differ from values obtained if only single scattered photons are taken into account (Wang 2002, Bykov *et al* 2005). Also for Doppler OCT, simulated flow profiles have been found to be distorted (Lindmo *et al* 1998). Since MC simulations determine the optical properties on a photon by photon basis, independent scattering is assumed and concentration-dependent scattering effects cannot be taken into account. Consequently, only for low scattering coefficients, where the linear relation between scattering coefficient and concentration holds, MC simulations can be quantitatively compared to calculated scattering coefficients.

In this study, we investigate the effect of multiple scattering on the Doppler OCT measurements of flowing blood by comparing the measurements to MC simulations. We take the following steps.

- (i) Doppler OCT measurements are performed on flowing blood with varying hematocrit (HCT). HCT and mean cell volume (MCV) of the samples are measured after the experiment.
- (ii) The MCV is used as an input parameter for discrete dipole approximation (DDA) calculations yielding the scattering cross section and phase function of a RBC in a particular orientation. The HCT is used to calculate the scattering coefficient from the scattering cross section.
- (iii) The orientation-averaged scattering coefficient and phase function are calculated and used in MC simulations of the Doppler OCT signals.
- (iv) For HCT < 10%, Doppler OCT measurements are compared to the MC simulations. MC simulations are based on a parabolic flow profile and constant scattering coefficient across the flow channel.

Our work explains the relatively low attenuation coefficient of blood measured with OCT and the relatively well-preserved flow profiles in Doppler OCT on blood.

2. Materials and methods

2.1. Spectral-domain Doppler OCT

We use a homemade Doppler OCT system (Kalkman *et al* 2010) operating at a center wavelength of $\lambda = 1300$ nm, with a 40 nm bandwidth ($\approx 18 \mu\text{m}$ axial resolution). The measured

OCT signal amplitude is corrected for the signal background, system depth sensitivity and the confocal point spread function of the focusing lens (Rayleigh length = 1.2 mm) (van Leeuwen *et al* 2003). Optical path lengths are converted to physical depth by dividing the optical path length with an effective refractive index based on the relative concentrations of water ($n = 1.33$ (Daimon and Masumura 2007)) and hemoglobin ($n = 1.40$, extrapolated from Friebel and Meinke (2005)). The OCT signal attenuation coefficient is determined by a two-parameter single exponential fit (attenuation rate μ_{OCT} and amplitude) over a range in the cuvette where the signal shows a single exponential decay. Since in OCT, the signal mapped to depth z corresponds one to one to the path length the light has traveled, this light is attenuated by absorption according to $\exp(-\mu_a z)$. Consequently, the fitted OCT attenuation coefficient μ_{OCT} is corrected for absorption by subtraction of the HCT-dependent μ_a and in this way we obtain the OCT attenuation coefficient due to scattering only, which we call $\mu_{\text{OCT},s}$. The absorption at 1300 nm wavelength for pure water is $\mu_a = 0.135 \text{ mm}^{-1}$ (Hale and Query 1973) and $\mu_a = 0.28 \text{ mm}^{-1}$ for hemoglobin at HCT = 5% (Roggan *et al* 1999). Standard deviations of the measured OCT quantities are calculated from five sequential measurements.

A flow cuvette with a 0.5 mm thick flow channel of rectangular cross section is made from MgF₂. MgF₂ has a rather low refractive index of $n = 1.38$ at 1300 nm (Bass 1994), thereby reducing the strong reflection at the interface between the blood and glass. The cuvette is mounted vertically to ensure that gravity, if it has any effect on the flow, is constant across the flow channel. Doppler flow measurements are performed at $75^\circ \pm 1^\circ$ relative to the plane of the cuvette. Due to refraction at the air/glass and glass–blood interfaces, the corresponding Doppler angle in the medium is $80^\circ \pm 1^\circ$. The measured Doppler frequencies are converted to flow using the Doppler angle in the medium, the refractive index of the medium and the wavelength.

Flow is generated with a perfusion pump (Perfusor fm, B Braun). The flow is set at 100 ml h^{-1} , but varies 10% in time. The average flow velocity is $5.5 \pm 0.8 \text{ mm s}^{-1}$ at the position of the measurement window. The calculated shear rates range between 0 and $33 \pm 5 \text{ s}^{-1}$.

To demonstrate the distortion of the measured flow profile, the Doppler flow profile is fitted between the borders of the cuvette with two functions. First, a parabola with $f_{\text{Dopp}}(z) = f_{\text{max}}(1 - (1 - (z/r))^2)$ is fitted, with z being the distance from the first interface and r half the width of the flow cuvette. Second, a five-parameter polynomial with $f_{\text{Dopp}}(z) = a_1 z + a_2 z^2 + a_3 z^3 + a_4 z^4 + a_5 z^5$ is fitted, with a_i being a fit parameter.

Fresh porcine blood is drawn and anti-coagulated before use. It is washed, centrifuged at 3500 rpm, and the supernatant is replaced with phosphate buffered saline. Dilutions of the initial solution are made by adding phosphate buffered saline to the solution. For each solution, a sample is taken right after the Doppler OCT measurement and analyzed with an XE-5000 automated hematology system to determine the MCV and HCT. Doppler OCT measurements are performed for RBC concentrations up to HCT = 15% since this is the highest concentration at which an OCT signal from the backside of the cuvette can be measured.

2.2. DDA calculations

The scattering cross section of a RBC is estimated using the DDA, calculated with the ADDA code (Yurkin *et al* 2007). Calculations are performed for $\lambda = 1300 \text{ nm}$ using the RBC's dimensions determined from the MCV as an input parameter (see table 1). The RBCs are modeled by oblate spheroid particles, this shape being the simplest non-spherical approximation for the RBC. The refractive index of the medium is estimated at $n_{\text{med}} = 1.33$. For the refractive index contrast ratio, we choose $|m| = 1.05$ (Friebel and

Table 1. Hematocrit and mean cell volume (MCV) for the porcine blood dilutions used in the experiments.

Hematocrit (vol%)	MCV (fL)
15	71.8
11	74.2
8	74.8
5	74.6
2.5	76.9
1	78.6

Meinke 2005). The ratio of the short- over the long-axis lengths of the oblate spheroid is estimated to be 0.25 (Cardoso and Camargos 2002). As output of the DDA calculations, we obtain Mueller matrices for all scattering angles. For oblate spheroids, these Mueller matrices are calculated for two extreme orientations (short axis in the direction of the beam and short axis perpendicular to the beam). The M_{11} Mueller matrix elements (isotropic polarization scattering) are integrated over all scattering angles to obtain the scattering cross section and scattering anisotropy g . The scattering cross section σ_s is converted to μ_s using the concentration C derived from the measured HCT, MCV and the relation $\mu_s = C\sigma_s$. The average phase function $p(\theta)$ is calculated using the phase function $p_0(\theta)$, $p_{90}(\theta)$ and the scattering coefficients $\mu_{s,0}$, $\mu_{s,90}$ at the two extreme orientations (Kodach *et al* 2011), according to $p(\theta) = (\mu_{s,0}p_0(\theta) + \mu_{s,90}p_{90}(\theta))/(\mu_{s,0} + \mu_{s,90})$.

2.3. MC simulations

The absorption coefficient, the orientation-averaged scattering coefficient and the orientation-averaged phase function are used as input for the description of the blood scattering medium in the MC simulation. For the calculation of a single Doppler OCT A-line, the trajectories of a large number of photons are generated and analyzed. The incoming photons are modeled in the form of a pencil beam. Photons are assumed coherent if their single pass optical path length is within half a coherence length of their maximum depth (weighted by a Gaussian). The outgoing coherent photons are detected using a Gaussian beam geometry with a finite size detector located at the focal distance from the flowing blood. The Doppler OCT signal is simulated only for the region that contains scatterers. More details on the MC code and the OCT signal simulation can be found in Bykov *et al* (2005).

3. Results

3.1. OCT signal attenuation and Doppler profile

Figure 1 shows the Doppler OCT measurements for three HCT values. The Doppler OCT measurements have been given an offset to facilitate comparison. Figure 1(a) shows the OCT attenuation as a function of depth. For all HCT, the OCT signal increases in the first $\approx 100 \mu\text{m}$ and then decreases with a single exponential decay toward the end of the cuvette. The OCT attenuation increases with HCT and is quantified with a single exponential fit of the OCT signal (see dashed line). At distances larger than the cuvette thickness, OCT signals can be observed. Since OCT signals from these distances do not correspond to locations of scatterers in the blood, this OCT signal is attributed to light that is multiple scattered in the cuvette and has acquired a longer path length. Figure 1(b) shows the Doppler OCT measurements as a function of depth. For low HCT, the Doppler profile is

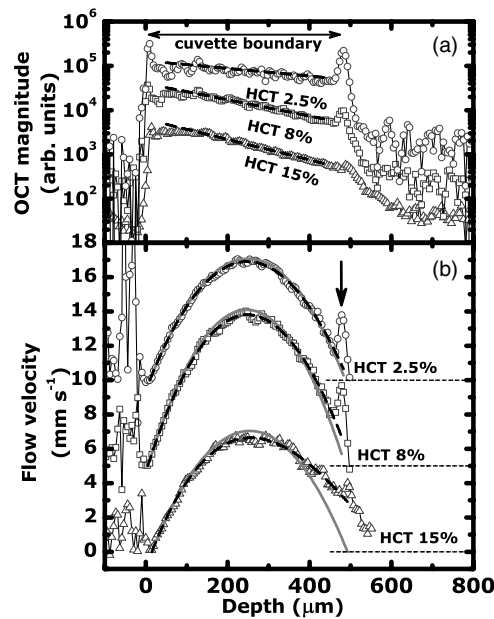


Figure 1. (a) OCT magnitude versus depth for three different HCT. The cuvette boundary is indicated and data are offset to facilitate comparison. (b) Doppler flow profiles for the same three HCT values. Data are shifted vertically with 5 and 10 mm s^{-1} for the HCT 8% and 2.5%, respectively. Parabolic and polynomial fits of the Doppler profile are overlaid on top of the data; the arrow indicates the reflection of forward scattered light at the blood/glass interface.

a perfect parabola, as expected for laminar blood flow at low flow speeds. A small peak can be observed at the backside of the cuvette, which is attributed to a large number of forward scattered light (high g) that reflects back from the blood/glass interface. For increasing HCT, the Doppler OCT flow profile becomes increasingly more asymmetric in shape and the signal-to-noise ratio at the backside decreases due to the higher optical attenuation. Most importantly, the measured Doppler frequency at the backside of the cuvette increases.

3.2. Comparison of OCT scattering coefficient and DDA calculations

Figure 2(a) shows $\mu_{\text{OCT},s}$ obtained from the data in figure 1(a) and at the other HCT levels. The OCT scattering coefficient increases with HCT as expected, but the attenuation coefficient levels off at about 5 mm^{-1} for HCT = 15%. Also indicated is the HCT = 10% boundary and the linear dependence of $\mu_{\text{OCT},s}$ for HCT between 0% and 10%. Figure 2(b) shows the same data as in figure 2(a) on a log scale and the DDA calculations. The dark gray band shows the range of scattering coefficients for the two extreme orientations of the oblate spheroid, short axis in the direction of the beam (lower limit) or short axis perpendicular to the beam (upper limit). The circles and solid line represent the average of the two orientations. Most importantly, the calculated values for the scattering coefficient are significantly higher for both extreme orientations $\mu_{\text{OCT},s}$. For very low HCT, the difference between the calculated scattering coefficient and $\mu_{\text{OCT},s}$ decreases. Finally, also indicated is the scattering coefficient determined by Roggan *et al* (1999).

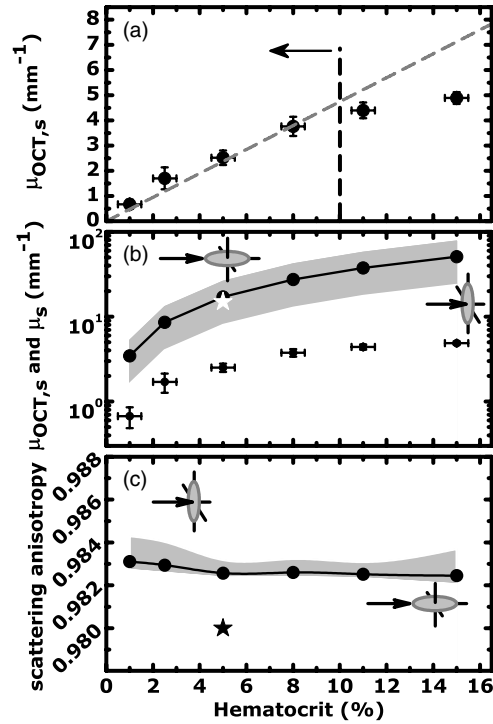


Figure 2. (a) Measured OCT attenuation coefficients. Indicated is the linear relation between the OCT attenuation coefficient for $HCT < 10\%$ (boundary indicated). (b) Comparison between the OCT scattering coefficient and the calculated scattering coefficients for oriented oblate spheroids (upper and lower limits of the shaded boundary, orientation indicated) and orientation-averaged oblate spheroids (circles and solid black line). The value of μ_s for human RBCs is indicated with a star (Roggan *et al* 1999). (c) Calculated scattering anisotropy g for oriented oblate spheroids (upper and lower limits of the shaded boundary, orientation indicated) and orientation-averaged oblate spheroids (circles and solid black line). The value of g for human RBCs is indicated with a star (Roggan *et al* 1999).

3.3. Comparison of Doppler OCT measurements to MC simulations

A comparison between Doppler OCT measurements and MC simulations is performed for $HCT = 8\%$. This is the highest measured HCT below $HCT = 10\%$ for which the linear relation between scattering coefficient and concentration holds (see figure 2(a), Steinke and Shepherd (1986) and Meinke *et al* (2007)) and avoids any concentration-dependent scattering effects. Figure 3 shows the Doppler OCT measurements for $HCT = 8\%$, compared to MC simulations calculated with $\mu_s = 27 \text{ mm}^{-1}$ (from figure 2), $\mu_a = 0.37 \text{ mm}^{-1}$ and the orientation-averaged phase function. The OCT and Doppler OCT signals are normalized and compared to the MC simulation. MC simulations are shown for the sum of all detected photons and for contributions according to the number of scattering events N a photon has experienced. The increasing OCT signal at the first glass/blood interface and the slope of the OCT signal as well as the small peak at the second blood/glass interface are well reproduced by the MC simulation. As can be seen, higher scattering orders are mainly deeper in the sample, and the rise in the first $100 \mu\text{m}$ is due to the buildup of higher scattering order signals deeper in the sample. At the backside of the cuvette, most photons have experienced more than 20 scattering events. The decay of the OCT signal as a function of depth is much smaller than predicted by the single scattering model, i.e. $\mu_{OCT,s} = 3.8 \text{ mm}^{-1}$ versus $\mu_s = 27 \text{ mm}^{-1}$.

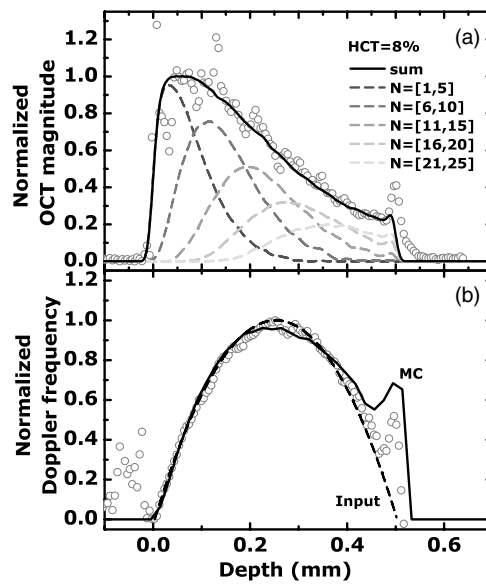


Figure 3. (a) OCT data of figure 1(a) for HCT = 8% (circles), MC simulation for the sum over all photons (black solid line), and for different scattering orders (see legend). (b) Doppler OCT data of figure 1(b) for HCT = 8% (circles), MC simulation (black solid line) and single scattering model (gray dashed line).

The MC simulation of the Doppler OCT flow profile matches the measured flow profile and is close to the single scattering model parabolic flow profile. The increase of the Doppler frequency at the second blood/glass interface is reproduced by the MC simulations albeit that the distortion of the MC simulated flow profile is larger than measured. At this HCT, the Doppler OCT flow profile clearly deviates, albeit by a small amount, from a parabola, especially at the back end of the cuvette. For Doppler OCT measurements with HCT smaller than 8%, similar agreement between Doppler OCT measurements and MC simulations is observed, with the deviation between the single scattering model and the measurements being smaller (data not shown).

4. Discussion

4.1. Results

The main result of our work is twofold: first, the Doppler OCT measurements show OCT attenuation coefficients $\mu_{\text{OCT},s}$ that are between a factor 5 to 10 lower than the calculated scattering coefficients μ_s ; second, the Doppler OCT measurements show a relatively small difference compared to the single scattering parabolic flow profiles. Limiting the comparison between Doppler OCT and MC simulations to HCT < 10%, we observe good agreement between our Doppler OCT measurements and MC simulations based on the optical parameters determined from DDA calculations. The initial increase of the OCT signal in the first region (up to around 100 μm) is due to the buildup of higher scattering orders in depth. The slope of the OCT signal is much lower than that predicted by the single scattering model. Therefore, multiple scattering increases the detected OCT signal, especially for scatterers with high g such as RBCs. We hypothesize that due to the low scattering angle (high g) photons scatter very

little in the lateral direction. Therefore, even when photons are scattered multiple times, the majority of photons stay in the beam. Consequently, the attenuation of light is much smaller, as is observed in the experiments. Figure 3(a) shows that at the backside of the cuvette the majority of photons has scattered more than 20 times. The small peak originating from photons reflected from the backside is also reproduced by the MC simulation albeit the simulated peak is a little bit smaller.

For the Doppler OCT flow measurements, the MC simulation shows a stronger deviation at large depth from the single scattering parabolic flow profile. We attribute this to small deviations in the true RBC phase function compared to the one that was used in the simulations. A deviation of the Doppler OCT flow profile from the single scattering parabola due to multiple scattering was observed in other studies. Cimalla *et al* (2011) used blood flowing through a square cross section glass cuvette, similar to our experimental geometry, and observed both the deviation in the flow profile and the peak at the backside. Others observed the deviation of the flow profile, but did not observe the peak at the second interface because the Doppler angle was too large (Moger *et al* 2005) or the flow was measured *in vivo* with a low-index contrast blood/wall interface (Yazdanfar *et al* 2000).

In this work, we presented a simple model to calculate the RBC properties and use these as input for MC simulations of the Doppler OCT signal. We operate in a shear rate regime where the shape of the RBC and its spatial distribution in the flow channel are not strongly affected (Moger *et al* 2004), justifying our assumptions for a constant scattering coefficient across the flow channel and oblate spheroid with a constant aspect ratio. Absolute OCT magnitude and absolute flow quantification are improvements that can be made to further improve the simulation=measurement comparison. Obviously, calculations of the optical properties of RBCs can be improved by taking into account the more complex shape of RBCs (true RBC shape versus ellipsoid), size variation (measured RBC distribution width $\approx 16\%$) and/or a better defined orientation (oriented RBCs). Although these improvements may result in slightly different results, we observed that these variations do not significantly change the main results presented in this work. In contrast, our calculations as shown in figures 2(b) and (c) closely match the values measured by Roggan *et al* (1999). Furthermore, extending the analysis to HCT $> 10\%$ is interesting. However, concentration-dependent scattering effects are difficult to model as they depend on the RBC shape, orientation and spatial distribution.

4.2. Doppler OCT signals for varying g

Compared to the single scattering description of the OCT signal, multiple scattering effects decrease the attenuation of the OCT signal in depth and affect the Doppler OCT flow profile at large depths. In general, these multiple scattering effects increase with increasing scattering coefficient. However, the effect of g on the Doppler OCT signal is more complicated. Figure 4 shows MC simulations for our experimental geometry using a scattering coefficient $\mu_s = 5 \text{ mm}^{-1}$, $\mu_a = 0 \text{ mm}^{-1}$ and varying g (phase function calculated with a Henyey–Greenstein phase function). Figure 4(a) shows that the slope of the OCT signal decreases with increasing g due to increasing amounts of multiple scattered photons in the OCT signal. For $g = 0$, the slope of the OCT signal attenuation is close to that described by the single scattering model; for this g , multiple scattering effects are small. For increasing g , a significant decrease of the slope of the OCT signal can be observed with increasing g , in agreement with our observations for blood. This is further indicated in the inset where the single exponential part of the decay is fitted and the slope is plotted against g . Figure 4(b) shows MC simulations of the Doppler OCT flow profiles at three different scattering anisotropies.

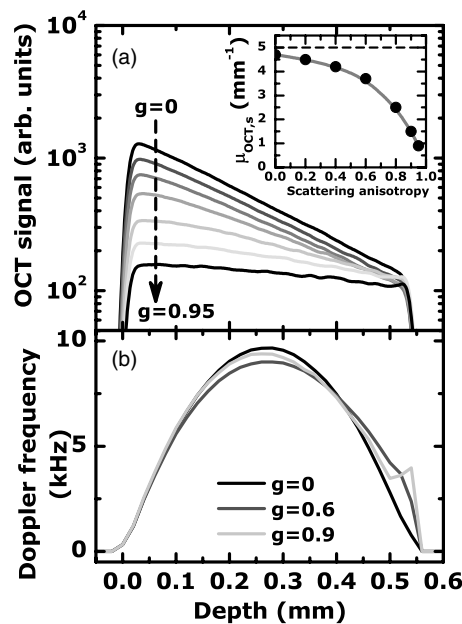


Figure 4. (a) MC simulations of the OCT signal in depth for varying scattering anisotropy g (calculated at g values indicated in the inset). As g increases, the slope of the OCT signal decreases due to increasing amounts of multiple scattering in the OCT signal. The inset shows the slope of the OCT signal for varying g . (b) Doppler OCT flow profiles at selected g values (indicated). At $g = 0.6$, the distortion of the flow profile is highest; at both very high and very low g the distortion of the Doppler OCT flow profile is low.

For $g = 0$, the input flow profile is very accurately reproduced because the Doppler OCT signal is formed mostly by the single scattered photons. For $g = 0.6$, the flow profile is significantly distorted, and finally for $g = 0.95$, the flow profile again is distorted very little; however, for this g , the contribution of multiply scattered photons in this case is significant (see figures 3 and 4(a)).

We attribute this effect to the interplay between Doppler shift per scattering event and the number of scattering events. For very low g , the Doppler shift per scattering event is very large; however, these photons are very rapidly scattered sideways out of the focused Gaussian beam and do not contribute to the OCT signal. On the other hand, for very high g , the photons are mainly forward scattered and stay in the beam. However, strictly forward scattered photons (zero scattering angle) do not gain any Doppler shift, and their Doppler shift is only determined by the backscattering event that brings them back into the focusing lens. Therefore the effect of multiple scattering on the measured Doppler OCT flow profile is largest at intermediate $g \approx 0.6$ where a significant fraction of the detected light is multiple scattered and these multiple scattered photons also experience a significant Doppler shift per scattering event. Forward scattering also leads to the appearance of a small peak at the backside interface of the Doppler OCT flow profile (as can be seen from figure 4(b)), even though the specularly reflected beam does not hit the detector (the capillary is tilted relative to the probing beam). This peak is attributed to multiple scattered photons that reflect on the blood/glass interface, which is why it is not present in the case when only single scattering is present.

5. Conclusion

Our measurements, calculations and simulations explain the relatively low attenuation coefficients and well preserved flow profiles measured with Doppler OCT on flowing blood. For blood with HCT < 15%, the OCT attenuation coefficient is a factor of 5–10 lower compared to the single scattering coefficient. The Doppler OCT profile for these measurements shows a relatively small distortion from the single scattering parabolic flow profile. From the comparison between Doppler OCT measurements and the MC simulations, we conclude that multiple scattering has a strong effect on the OCT signal attenuation in depth, but a relatively weak effect on the Doppler OCT flow profile. We predict that distortions of the Doppler OCT flow profiles are strongest at large depths in the sample, for samples with high scattering coefficients, and samples with intermediate scattering anisotropy ($g \approx 0.6$).

Acknowledgments

We thank R H Bremmer for useful discussions. J Kalkman is supported by the IOP Photonic Devices program (IPD067774) managed by the Technology Foundation STW and SenterNovem. A V Bykov acknowledges Finnish Funding Agency for Technology and Innovation (Tekes), FiDiPro project, no. 1027 21 2010.

References

- Bass E M 1994 *Handbook of Optics* vol 2 (New York: McGraw-Hill)
- Bykov A V, Kirillin M Yu and Priezhev A V 2005 Monte Carlo simulation of an optical coherence Doppler tomograph signal: the effect of the concentration of particles in a flow on the reconstructed velocity profile *Quantum Electron.* **35** 135
- Cardoso A V and Camargos A O 2002 Geometrical aspects during formation of compact aggregates of red blood cells *Mater. Res.* **5** 263
- Chen Z, Milner T E, Srinivas S, Wang X, Malekafzali A, van Gemert M J C and Nelson J S 1997 Noninvasive imaging of *in vivo* blood flow velocity using optical Doppler tomography *Opt. Lett.* **22** 1
- Cimalla P, Walther J, Mittasch M and Koch E 2011 Shear flow-induced optical inhomogeneity of blood assessed *in vivo* and *in vitro* by spectral domain optical coherence tomography in the 1.3 μm wavelength range *J. Biomed. Opt.* **16** 106020
- Daimon M and Masumura A 2007 Measurement of the refractive index of distilled water from the near-infrared region to the ultraviolet region *Appl. Opt.* **46** 3811
- Faber D J and van Leeuwen T G 2009 Are quantitative attenuation measurements of blood by optical coherence tomography feasible? *Opt. Lett.* **34** 1435
- Friebel M and Meinke M 2005 Determination of the complex refractive index of highly concentrated hemoglobin solutions using transmittance and reflectance measurements *J. Biomed. Opt.* **10** 06419
- Hale G M and Querry M R 1973 Optical constants of water in the 200-nm to 200- μm wavelength region *Appl. Opt.* **12** 555
- Huang D *et al* 1991 Optical coherence tomography *Science* **254** 1178
- Izatt J A, Hee M R, Owen G M, Swanson E A and Fujimoto J G 1994 Optical coherence microscopy in scattering media *Opt. Lett.* **19** 590
- Kalkman J, Bykov A V, Faber D J and van Leeuwen T G 2010 Multiple and dependent scattering effects in Doppler optical coherence tomography *Opt. Express* **18** 3883
- Kodach V M, Faber D J, van Marle J, van Leeuwen T G and Kalkman J 2011 Determination of the scattering anisotropy with optical coherence tomography *Opt. Express* **19** 6131
- Lindmo T, Smithies D J, Chen Z, Nelson J S and Milner T E 1998 Accuracy and noise in optical Doppler tomography studied by Monte Carlo simulation *Phys. Med. Biol.* **43** 3045
- Meinke M, Müller G, Helfman J and Friebel M 2007 Empirical model functions to calculate hematocrit-dependent optical properties of human bloods *Appl. Opt.* **46** 1742

- Moger J, Matcher S J, Winlove C P and Shore A 2004 Measuring red blood cell flow dynamics in a glass capillary using Doppler optical coherence tomography and Doppler amplitude optical coherence tomography *J. Biomed. Opt.* **9** 982
- Moger J, Matcher S J, Winlove C P and Shore A 2005 The effect of multiple scattering on velocity profiles measured using Doppler OCT *J. Phys. D: Appl. Phys.* **38** 2597
- Roggan A, Friebel M, Dörschel K, Hahn A and Müller G 1999 Optical properties of circulating human blood in the wavelength range 400-2500 nm *J. Biomed. Opt.* **4** 36
- Steinke J M and Shepherd A P 1986 Role of light scattering in whole blood oximetry *IEEE Trans. Biomed. Eng.* **33** 294
- van Leeuwen T G, Faber D J and Aalders M C 2003 Measurement of the axial point spread function in scattering media using single-mode fiber-based optical coherence tomography *IEEE J. Sel. Top. Quantum Electron.* **9** 227
- Wang R K 2002 Signal degradation by multiple scattering in optical coherence tomography of dense tissue: a Monte Carlo study towards optical clearing of biotissues *Phys. Med. Biol.* **47** 2281
- Yazdanfar S, Rollins A M and Izatt J A 2000 Imaging and velocimetry of the human retinal circulation with color Doppler optical coherence tomography *Opt. Lett.* **25** 1448
- Yurkin M A, Maltsev V P and Hoekstra A G 2007 The discrete dipole approximation for simulation of light scattering by particles much larger than the wavelength *J. Quant. Spectrosc. Radiat. Transfer* **106** 546